

Relativistic Astronomy. II. In-Flight Solution of Motion and Test of Special Relativity Light Aberration

JIN-PING ZHU,¹ BING ZHANG,^{2,1,3} AND YUAN-PEI YANG^{4,3}

¹*Department of Astronomy, School of Physics, Peking University, Beijing 100871, China; zhujp@pku.edu.cn*

²*Department of Physics and Astronomy, University of Nevada Las Vegas, NV 89154, USA; zhang@physics.unlv.edu*

³*National Astronomical Observatories, Chinese Academy of Sciences, Beijing 100012, China*

⁴*Kaoli Institute for Astronomy and Astrophysics, Peking University, Beijing 100871, China*

Submitted to ApJ

ABSTRACT

The Breakthrough Starshot project aims to send centimeter-sized, gram-scale “StarChip” probes to Alpha Centauri at a speed of $\sim 0.2c$. On the other hand, Zhang & Li recently proposed that trans-relativistic cameras may be sent to any direction to study astronomical objects and test special relativity. To conduct such “relativistic astronomy”, one needs to solve the motion of the probe in flight. We solve the motion of the probe (including the moving direction and the velocity) by comparing the positions of three or more point sources observed in the Earth rest frame and in the probe’s comoving frame. When the positions of enough point sources are taken into account, the motion of the probe can be solved with an error which is even smaller than the diffraction limit of the transrelativistic camera. After solving the motion, when the measurement of the position of an additional point source is introduced, one can use the data to test the light aberration effect in special relativity. The upper limit of the photon mass can be placed from the deviation of aberration to slightly lower than the energy of the photon, e.g. $\sim 1\text{eV}$.

Keywords: methods: observational

1. INTRODUCTION

The Breakthrough Starshot is a program of the Breakthrough Initiatives¹ with the aim of proving the concept of developing ultra-fast light-driven probes. The centimeter-sized, gram-scale “StarChip” probes, each carrying 4 sub-gram-scale 2 megapixel cameras, are expected to be accelerated to a speed of $\sim 0.2c$, which is projected to reach Alpha Centauri in ~ 20 yr from the launch and transfer back to earth the images of the exoplanet Proxima b orbiting Proxima Centauri 4.37 ly away (Anglada-Escudé et al. 2016).

When a probe travels with a transrelativistic speed, some interesting relativistic effects can be observed. For example, Christian & Loeb (2017) presented a method of measuring acceleration of a probe using the temporal Terrell effect (Terrell 1959; Penrose 1959). To perform such measurements, the probe needs to be close to astrophysical masses, so that the size of the objects can be measured.

Zhang & Li (2018) (Paper 1) suggested that one can actually use relativistic cameras more generally. Instead of aiming them to a particular target (e.g. Alpha Centauri), they suggested that one can send these cameras to any direction to study the universe. As natural spectrographs, lenses, and wide-field cameras, relativistic cameras can be used to observe the universe in an unprecedented manner and to perform unique tests on relativity. Zhang & Li (2018) termed this approach of studying the universe “relativistic astronomy”.

With a transrelativistic camera in space, one important task is to solve the motion of the camera (including both the direction of motion and the speed of the camera), so that the Doppler factors in all the directions in the sky can be solved precisely. One may use the information of the initial laser acceleration configuration or the telecommunication signals to determine these parameters. For a long enough observation, one can use the relative motion of the distant objects, i.e. the optical flow, to infer the motion of the probe. However, after acceleration is finished, the camera will

¹ <https://breakthroughinitiatives.org>

travel in the geodesic trajectory defined by the gravitational field of all the masses (e.g. Sun, Earth, Moon, and other large planets), so that both the direction and the speed of the camera are subject to change. The telecommunication method requires multiple receiving stations, and becomes progressively difficult as the probe travels far away from Earth. On the other hand, it is possible to use the in-flight “snapshot” image of some point sources and compare them with the image taken from Earth (Zhang & Li 2018). This paper addresses this problem in great detail and show that the motion of the camera can be indeed solved using the information of three or more point sources (Section 2).

A transrelativistic camera also allows a direct test of the light aberration effect in an unprecedented regime (Zhang & Li 2018). Hirshfeld (2001) tested aberration of light by observing the parallaxes of distant stars. Kopeikin & Fomalont (2007) measured a small gravitational aberration of light by Earth-based experiments. Due to the slow motion and weak gravity of the earth, the precision of these tests was limited. In this paper, we present a detailed treatment to perform more precise constraints on the deviation of the aberration angle in special relativity and a constraint on the rest mass of the photon by the aberration measurements (Section 3).

2. SOLVING THE MOTION OF A TRANSRELATIVISTIC CAMERA

2.1. Method

When a camera travels in the interstellar space with a transrelativistic speed, the positions of celestial objects will be more concentrated in the moving direction due to the relativistic effects. Suppose that a probe carrying a camera moves in a certain direction with a constant speed. One can define two rest frames: the Earth rest frame K , and the probe’s comoving frame K'^2 . Let us define the Lorentz factor of the probe as $\Gamma = 1/\sqrt{1-\beta^2}$, where $\beta = v/c$ is the normalized speed of the probe. The angle between the object moving direction and the line of sight in two different frames are related through the relation of light aberration (Rybicki & Lightman 1979):

$$\cos \theta' = \frac{\cos \theta + \beta}{1 + \beta \cos \theta}. \quad (1)$$

The parameters of the motion of the probe include the direction of motion and the dimensionless velocity β . In order to solve the motion of the probe, one needs to measure the sky positions of at least three point sources in Frame K' ($1'$, $2'$, $3'$) and compare them with the sky positions of the same three objects in Frame K (1 , 2 , 3) (see also Zhang & Li 2018). Let us suppose that the direction of motion is to the point 0 and $0'$ in Frame K and Frame K' , respectively. As seen from Figure 1, the sky positions of the sources in Frame K' are located at the great circles defined by their corresponding sources in Frame K and the direction of motion of the probe. As a result, the opening angle of spherical triangle with the direction of motion as the vertex is unchanged after relativistic transformation, e.g. $\angle 102 = \angle 1'0'2'$.

We first consider a bottom-up (forward) approach of the problem assuming that the probe motion is known. The steps of solving the geometry of a three-point-source problem include the following:

1. Measure the parameters that define the direction of motion (i.e., right ascension α_0 and declination δ_0 in the equatorial coordinate system) in Frame K and the positions of the three point sources (i.e., α_i , δ_i , $i = 1, 2, 3$).
2. Use Eq.(A1) (see Appendix A.1) to obtain the angles between the direction of motion and three point sources in Frame K (i.e., θ_{01} , θ_{02} and θ_{03}) as well as the angles between three point sources themselves in Frame K (i.e., θ_{12} , θ_{13} and θ_{23}).
3. Use Eq.(1) to obtain the angles between the direction of motion and the three point sources in Frame K' (i.e., $\theta'_{0'1'}$, $\theta'_{0'2'}$ and $\theta'_{0'3'}$).
4. Use Eq.(A2) (see Appendix A.2) to obtain $\angle 102$, $\angle 103$ and $\angle 203$ in Frame K . The angles $\angle 1'0'2'$, $\angle 1'0'3'$ and $\angle 2'0'3'$ in Frame K' are equal to $\angle 102$, $\angle 103$ and $\angle 203$ in Frame K , respectively.
5. Use Eq.(A2) (see Appendix A.2) to obtain the angles between the three point sources themselves in Frame K' (i.e., $\theta'_{1'2'}$, $\theta'_{1'3'}$ and $\theta'_{2'3'}$).

² More precisely, one should use the barycenter rest frame of the solar system rather than the Earth frame for the rest frame K . This will introduce an additional small correction factor scaled with the Earth motion speed ($\beta \sim 10^{-4}$), which is much smaller than the probe’s motion speed. Also since we care about the snapshot images taken from both frames, the optical flow effect can be neglected.

Next, we consider a top-down (inverse) approach, in which we use the observed quantities to infer the information of motion, including the direction of motion (i.e., α_0, δ_0) and the dimensionless velocity β . We start with three point sources as an example. In practical observations, one can only obtain the positions of the three point sources with certain observational uncertainties in both Frame K (i.e., $\alpha_i, \delta_i, i = 1, 2, 3$, and $\sigma_{\alpha_i}, \sigma_{\delta_i}$) and Frame K' (i.e., $\alpha'_i, \delta'_i, i' = 1, 2, 3$, and $\sigma_{\alpha'_i}, \sigma_{\delta'_i}$). Using Eq.(A2) (see Appendix A.2), one can obtain the corresponding angles in Frame K' (i.e., $\theta'_{1'2'}, \theta'_{1'3'}$ and $\theta'_{2'3'}$). The covariance error tensor $\sigma'_{\theta'}$ can be obtained by error propagation since $\theta'_{1'2'}$, $\theta'_{1'3'}$ and $\theta'_{2'3'}$ depend on $\alpha'_1, \delta'_1, \alpha'_2, \delta'_2, \alpha'_3$ and δ'_3 in Frame K' . One can also define an observational-value vector $\boldsymbol{\theta} = [\theta'_{1'2'}, \theta'_{1'3'}, \theta'_{2'3'}]^T$. In order to calculate the position of the moving direction (i.e., α_0, δ_0) and the dimensionless velocity β , one can try different model values based on the bottom-up (forward) approach and compare them against the data. The χ^2 can be defined as

$$\chi^2 = (\boldsymbol{\theta} - \tilde{\boldsymbol{\theta}}) \sigma'_{\theta'}{}^{-1} (\boldsymbol{\theta} - \tilde{\boldsymbol{\theta}}), \quad (2)$$

where $\tilde{\boldsymbol{\theta}} = [\tilde{\theta}'_{1'2'}, \tilde{\theta}'_{1'3'}, \tilde{\theta}'_{2'3'}]^T$ is the theoretical-value vector. Going through a grid of the trial values of the moving direction (i.e., α_0, δ_0) and the dimensionless velocity β repeatedly, one can derive $\tilde{\theta}'_{1'2'}$, $\tilde{\theta}'_{1'3'}$ and $\tilde{\theta}'_{2'3'}$ for each trial, and use optimization algorithms, such as the Simulated Annealing algorithm (Metropolis et al. 1953; Kirkpatrick et al. 1983; Ingber 1989), to find the minimum χ^2 and identify the parameter optimum.

After solving the motion with three point sources, one can apply error propagation to calculate the uncertainty of each parameter, i.e., $\sigma_{\alpha_0}, \sigma_{\delta_0}, \sigma_{\beta}$, and the correlation coefficient between each pair of the parameters, i.e., $\rho_{\alpha_0\delta_0}, \rho_{\alpha_0\beta}, \rho_{\delta_0\beta}$. The angles $\theta'_{1'2'}$, $\theta'_{1'3'}$ and $\theta'_{2'3'}$ depend on $\alpha_0, \delta_0, \alpha_1, \delta_1, \alpha_2, \delta_2, \alpha_3, \delta_3, \beta$, which we assume that there is no correlation among the observational error of each parameter in Frame K . Then, the corresponding covariance matrix $\boldsymbol{\sigma}_{\theta'}$ of $\theta'_{1'2'}$, $\theta'_{1'3'}$ and $\theta'_{2'3'}$ in Frame K' can be obtained. On the other hand, we have obtained the covariance error tensor $\sigma'_{\theta'}$ when we calculate the parameter optimum. If $\boldsymbol{\sigma}_{\theta'}$ and $\sigma'_{\theta'}$ are similar (i.e., the three eigenvalues of $\boldsymbol{\sigma}_{\theta'}$ are equal to the three eigenvalues of $\sigma'_{\theta'}$, respectively), one can obtain the optimum of $\sigma_{\alpha_0}, \sigma_{\delta_0}, \sigma_{\beta}, \rho_{\alpha_0\delta_0}, \rho_{\alpha_0\beta}$ and $\rho_{\delta_0\beta}$.

2.2. An example

In the following, we use an example to show how one can use real data to solve the motion of a transrelativistic probe. Consider a transrelativistic camera on board a probe, which is moving towards the direction of Proxima Centauri and Proxima b. One can estimate the position accuracy of the probe using the method described above.

We assume that the following parameters are independent variables, e.g., the dimensionless velocity β of the probe, the angle θ_c between the moving direction of the probe and the center of the camera's field of view in Frame K' , as well as the angular radius r of the field of view of the camera on board the probe. Our goal is to use the measured data to constrain β and θ_c and see whether the input values can be reproduced.

In Frame K , the datasets of the positions of bright celestial objects and their uncertainties can be directly obtained from the Data Release 2 (Gaia Collaboration et al. 2018) of the *Gaia* mission (Gaia Collaboration et al. 2016). More specifically, we select some sources with high precision ($\sigma_{\alpha}, \sigma_{\delta} \lesssim 1$ mas) and high brightness (G -band magnitude $G \lesssim 4$ mag). The astrometric parameters for the *Gaia* Data Release 2 sources that satisfy these criteria in the field of view of Proxima Centauri are presented in Table 1. On the other hand, in Frame K' , the uncertainties of the celestial positions are approximately defined by the diffraction limit:

$$\theta \approx 1.22 \frac{\lambda}{D} = 3.59'' \left(\frac{\lambda}{500 \text{ nm}} \right) \left(\frac{D}{3.5 \text{ cm}} \right)^{-1}, \quad (3)$$

where θ is the angular resolution of the probe camera, λ is the wavelength of light, and D is the lens' aperture. With $\lambda \sim 500$ nm (the peak wavelength of sun-like spectrum) and $D \sim 3.5$ cm (the size of the first prototype of Starshot cameras³), the uncertainties of the positions in Frame K' are $\sim 3.59''$.

Table 2 shows some examples of solving the motion of the probe using observational data. The first four columns are the input parameters, including the probe dimensionless velocity β , the angular radius of the probe's field of view r , the angle between the moving direction and the center of the camera's field of view θ_c , and the aperture of the transrelativistic camera. The fifth column lists the three HIP point sources chosen from the *Gaia* catalog listed in Table 1. The three sources are chosen near the edge of the field of view, and we require nearly the same angular distance between each pair of the three points. Our top-down (reverse) approach can reproduce the input parameters β and

³ <https://breakthroughinitiatives.org/News/12>

θ_c , with uncertainties σ_{α_0} , σ_{δ_0} , and σ_β for the direction parameters (α_0, δ_0) and the speed parameter β , respectively, listed in the next three columns.

We start with the fiducial parameter set with $\beta = 0.2$, $r = 30^\circ$ and $\theta_c = 0^\circ$. The uncertainties of the moving direction are constrained to a precision of $\sigma_{\alpha_0}, \sigma_{\delta_0} \sim 10^{2''}$ ($\sim 10^{-5}$ rad), and the uncertainty of the dimensionless velocity is $\sigma_\beta \sim 10^{-5}$. Compared with the uncertainties of *Gaia*'s positions ($\sigma_\alpha, \sigma_\delta \lesssim 1$ mas) and the uncertainties of the camera in the probe (which is limited by the diffraction limit $\sim 3.59''$), these uncertainties are larger (by a factor of $10^1 - 10^2$). We investigate how these uncertainties depend on the input parameters. We find that the dependences on β and θ_c are weak, while the dependence on r is significant. Basically, if one shrinks the field of view, the position uncertainty would increase. We also test the dependence on the aperture of the camera D . The uncertainty inversely scales with D as expected from the diffraction limit formula. We conclude that to achieve a better precision to solve the motion of the probe, cameras with a larger aperture D and a larger field of view r are preferred. The challenge of relativistic astronomy would be therefore trying to enlarge both D and r with the limited payload mass on the probe.

2.3. Solving the motion with more than three point sources

The position accuracy derived from three data points is typically much worse than the diffraction limit. We expect that the accuracy can be improved if one includes the information of more point sources. We further explore a method to solve the motion with $n \geq 3$ point sources based on the general method described in Section 2.1.

We use the *Monte Carlo* method to generate n point sources with the assumption that all the point sources (i.e., α_i and δ_i , $i = 1, 2, 3, \dots, n$) are located at the boundary of the probe's field of view. The fiducial parameter we set is $\beta = 0.2$, $r = 30^\circ$ and $\theta_c = 0^\circ$. We assume that the uncertainties of the positions in Frame K are $\sigma_{\alpha_i}, \sigma_{\delta_i} \sim 1$ mas, while the uncertainties of the positions in Frame K' are $\sigma_{\alpha'_i}, \sigma_{\delta'_i} \sim 3.59''$.

When we estimate the position accuracy of the probe, a Markov Chain Monte Method (MCMC) based on `emcee` package (Foreman-Mackey 2013) is adopted. The prior distributions of parameters are taken to be flat in the linear space. Since there are n point sources to solve the motion, the dimensions of the observational-value vector $\boldsymbol{\theta}$ and theoretical-value vector $\tilde{\boldsymbol{\theta}}$ becomes $n(n-1)/2$. The covariance error tensor $\boldsymbol{\sigma}'_{\theta'}$ becomes a $\frac{n(n-1)}{2} \times \frac{n(n-1)}{2}$ tensor. The objective function, i.e., log likelihood function, is therefore given by

$$\ln \mathcal{L} = -\frac{n(n-1)}{4} \ln 2\pi - \frac{1}{2} \det \boldsymbol{\sigma}'_{\theta'} - \frac{1}{2} (\boldsymbol{\theta} - \tilde{\boldsymbol{\theta}}) \boldsymbol{\sigma}'_{\theta'}^{-1} (\boldsymbol{\theta} - \tilde{\boldsymbol{\theta}}). \quad (4)$$

We run each case 50 times. The results for the cases from 3 to 7 point sources are presented in Table 3. The uncertainties of the moving direction (σ_{α_0} and σ_{δ_0}) and the dimensionless velocity (σ_β) have an obvious decrease trend (see Figure 2) as a function of the selected point source number n . The decay rates of uncertainties will gradually decrease as the selected point source number n increasing. The precision of $\sigma_{\alpha_0}, \sigma_{\delta_0}$ can be even smaller than the camera's diffraction limit $\sim 3.59''$ when $n > 5$ is selected. We conclude that the direction of motion of the probe can be determined to the diffractive limit, if a large enough number of point sources (typically 5 or more) are selected to solve the motion.

3. TESTS OF RELATIVISTIC LIGHT ABERRATION AND CONSTRAINTS ON THE PHOTON MASS

3.1. Tests of relativistic light aberration effect

With the motion of the probe solved, one can test special relativity light aberration formula by comparing the predicted position and the measured position (Zhang & Li 2018). Selecting some point sources in Frame K , one can use the rotation transformation (see Appendix B) to calculate its celestial coordinate positions in Frame K' . For the cases of using three point sources to solve the motion of the camera, the results of position accuracy of the fourth point source are listed in the last four columns of Table 2. The position uncertainties are generally $< 60''$. Similar to the constraints on the moving direction, the camera's field of view r and aperture D play the most important roles in determining the position precision. For different point sources with a similar angle θ_{04} between the fourth point and the moving direction in Frame K , the position uncertainties are similar.

If we use n point sources to solve the motion of the camera, one can take the $(n+1)^{\text{th}}$ point source to test the relativistic light aberration effect. We again use the *Monte Carlo* method to test how the precision of the test increases with n . After solving the motion, we randomly generate the $(n+1)^{\text{th}}$ point source near the boundary of the probe's field of view. The statistical results are presented in Table 3. The position uncertainties of the $(n+1)^{\text{th}}$ point source also have a similar decrease relationship with the motion uncertainties as a function of n . Its position uncertainties are typically smaller than the diffraction limit $\sim 3.59''$.

3.2. Constraints on the photon mass

One specific mechanism to cause deviation of the aberration angle from the value predicted by special relativity is to invoke a non-zero mass of the photon (de Broglie 1922, 1923, 1940; Proca 1936a,b,c,d, 1937, 1938). Many methods have been proposed to constrain the rest mass of the photon, e.g., the solar wind magnetic field (Ryutov 1997, 2007), Coulomb's law (Williams et al. 1971), low frequency electromagnetic wave detection (Schumann 1952), the frequency dependence of the speed of light (Lovell et al. 1964; Wu et al. 2016; Shao & Zhang 2017), and pulsar spin-down (Yang & Zhang 2017). In the following, we constrain the photon mass using the limit of light aberration deviation measured from a transrelativistic camera.

If the photon has a non-zero rest mass m_γ , the Lorenz-invariant dispersion is

$$E = h\nu = \sqrt{p^2 c^2 + m_\gamma^2 c^4}. \quad (5)$$

The group velocity for a photon is

$$v_g = \frac{\partial E}{\partial p} = c \sqrt{1 - \left(\frac{m_\gamma c^2}{h\nu}\right)^2} \simeq c \left[1 - \frac{1}{2} \left(\frac{m_\gamma c^2}{h\nu}\right)^2\right], \quad (6)$$

where the last derivation holds when $m_\gamma \ll h\nu/c^2 \approx 2.48$ eV for optical light. Then, the aberration formula (Rybicki & Lightman 1979) becomes

$$\tan \theta' = \frac{v_g \sin \theta}{\Gamma(v_g \cos \theta + \beta c)}, \quad (7)$$

$$\cos \theta' = \frac{v_g \cos \theta + \beta c}{\sqrt{(v_g + \beta c \cos \theta)^2 + \beta^2 \sin^2 \theta (c^2 - v_g^2)}}, \quad (8)$$

For the case of $v_g = c$ (i.e., $m_\gamma = 0$), Eq.(8) becomes the light aberration formula in special relativity, i.e., Eq.(1).

Suppose that we can obtain two images of the same sky area independently photographed by an Earth-based telescope in Frame K and by a transrelativistic camera in Frame K' . Let us consider $n + 1$ point sources that are well measured in both K and K' . One can select n of the $n + 1$ point sources to solve the parameters of motion under the assumption of zero mass of the photon based on the method discussed in Section 2. In theory, the position of the $(n + 1)^{\text{th}}$ point source in Frame K' can be calculated. Therefore, one can obtain a theoretical image ‘‘photographed’’ by the transrelativistic camera. Matching the n point sources in the observed image that are used to solve the motion with the n corresponding point sources in the theoretical image, one can compare the position of the $(n + 1)^{\text{th}}$ point source between observed image and the theoretical image in Frame K' . If the photon mass is non-zero, one would expect a slight deviation of the $(n + 1)^{\text{th}}$ point source in two images due to the slight difference in the formulae of aberration of light. This is because the solution of motion and the angle between the direction of motion and $(n + 1)^{\text{th}}$ point in Frame K' would have been slightly different from the zero-photon-mass case. Using the upper limit on the mismatch between the $(n + 1)^{\text{th}}$ point source of the two images, one can set an upper limit on the mass of the photon.

We directly use the results of Section 2.3 to constrain the photon mass. Each run can obtain the uncertainties of the position of the $(n + 1)^{\text{th}}$ point source in Frame K' under the assumption of zero mass of the photon. Next, we assume a non-zero photon mass and then solve the motion using the m_γ aberration formula Eq.(8) to obtain the corresponding moving direction and dimensionless velocity. The position of the $(n + 1)^{\text{th}}$ point source can be correspondingly calculated. By comparing this position with the case of non-zero photon mass, one can obtain the upper limit on the mass of the photon by requiring that the deviation between the two cases exceeds the position uncertainty of the $(n + 1)^{\text{th}}$ point source. With the number of selected point sources increasing to solve the motion, the limit on the photon mass is tighter. For the case of $n = 7$, the upper limit of photon mass is constrained to ~ 0.3 eV. On the other hand, it won't become significantly lower than 1 eV defined by the energy of the optical band. This value is much greater than the maximum photon energy obtained using other methods (e.g. Ryutov 1997, 2007; Williams et al. 1971; Schumann 1952; Lovell et al. 1964; Wu et al. 2016; Shao & Zhang 2017; Yang & Zhang 2017). Hence, optical relativistic imagery is not particularly useful in constraining the photon mass.

4. CONCLUSIONS

In this paper, we present a detailed procedure to solve the motion of a transrelativistic camera using in-flight observational data. By comparing the positions of three sources observed in the Earth rest frame and in the probe's comoving frame, one can solve the motion of the probe including the direction and the velocity. We give some examples to show how one can use real data to solve the motion of the probe and estimate the precision of the motion with three point sources. By investigating the effect of the input parameters on the uncertainties of the motion, we conclude that a larger aperture and a larger field of view can give a better precision in solving the motion.

We further explore the approach to solve the motion with more than three point sources. By randomly generating point sources, we estimate the motion precision by an MCMC method. The precision increases with the increasing number of the selected point sources. The uncertainty of the moving direction can exceed the diffraction limit ($\sim 3.59''$), but would converge as n is more than 5.

With the motion of the probe solved, one can test the light aberration effect in special relativity. For the simplest case of using three point sources to solve the motion problem, the position uncertainty of fourth point source is typically smaller than that of the moving direction. Again the camera's field of view and aperture play the most important roles in defining the position precision. We also investigate how n point sources can improve the test. The uncertainty of the $(n + 1)^{\text{th}}$ point source also decreases with an increasing n , which is typically smaller than the diffraction limit $\sim 3.59''$.

The existence of the photon mass would introduce a slight difference in the formula of aberration of light. It causes a slight deviation of the position of $(n + 1)^{\text{th}}$ point source compared to the zero m_γ case. By requiring that the deviation of the position of $(n + 1)^{\text{th}}$ point source between the $m_\gamma \neq 0$ and $m_\gamma = 0$ to be smaller than the uncertainty of the position of $(n + 1)^{\text{th}}$ point source, one can place an upper limit on the photon mass. Our simulations show that the aberration method can constrain the photon mass to not too much below the photon energy 1 eV in the optical band. So this method is not competitive compared with other methods of constraining the photon mass.

The authors acknowledge anonymous referees for useful discussions. We also thank Rui Luo for helpful informations. This work is partially supported by the National Basic Research Program of China under grant No. 2014CB845800.

Software: Matlab, <https://www.mathworks.com>, Python, <https://www.python.org>, emcee (Foreman-Mackey 2013)

REFERENCES

- Anglada-Escudé, G., Amado, P. J., Barnes, J., et al. 2016, *Nature*, 536, 437
- Christian, P., & Loeb, A. 2017, *ApJL*, 834, L20
- de Broglie, L. 1922, *J. Phys. Radium*, 3, 422
- de Broglie, L. 1923, *Comptes Rendus Hebd. Séances Acad. Sc. Paris*, 177, 507
- de Broglie, L. 1940, *La Mécanique Ondulatoire du Photon. Une Nouvelle Théorie de la Lumière* (Paris: Hermann)
- Foreman-Mackey, D., Hogg, D. W., Lang, D., & Goodman, J. 2013, *PASP*, 125, 306
- Gaia Collaboration, Brown, A. G. A., Vallenari, A., et al. 2018, *A&A*, 616, A1
- Gaia Collaboration, Prusti, T., de Bruijne, J. H. J., et al. 2016, *A&A*, 595, A1
- Goldstein, H., Poole, C., & Safko, J. 2002, *Classical mechanics* (3rd ed.) by H. Goldstein, C. Poole, and J. Safko. San Francisco: Addison-Wesley, 2002
- Hirshfeld, A. W. 2001, *Parallax: The Race to Measure the Cosmos* (New York: Freeman)
- Ingber, A. L. 1989, *JMCM*, 12, 967
- Kirkpatrick, S., Gelatt, C. D., & Vecchi, M. P. 1983, *Science*, 220, 671
- Kopeikin, S. M., & Fomalont, E. B. 2007, *General Relativity and Gravitation*, 39, 1583
- Lovell, B., Whipple, F. L., & Solomon, L. H. 1964, *Nature*, 202, 377
- Metropolis, N., Rosenbluth, A. W., Rosenbluth, M. N., Teller, A. H., & Teller, E. 1953, *JChPh*, 21, 1087
- Proca, A. 1936a, *Comptes Rendus Hebd. Séances Acad. Sc. Paris*, 202, 1366
- Proca, A. 1936b, *Comptes Rendus Hebd. Séances Acad. Sc. Paris*, 202, 1490
- Proca, A. 1936c, *Comptes Rendus Hebd. Séances Acad. Sc. Paris*, 203, 709
- Proca, A. 1936d, *J. Phys. Radium*, 7, 347
- Proca, A. 1937, *J. Phys. Radium*, 8, 23
- Proca, A. 1938, *J. Phys. Radium*, 9, 61
- Penrose, R. 1959, *Proceedings of the Cambridge Philosophical Society*, 55, 137
- Perryman, M. A. C., Lindegren, L., Kovalevsky, J., et al. 1997, *A&A*, 323, L49

- Rybicki, G. B., & Lightman, A. P. 1979, New York, Wiley-Interscience, 1979. 393 p.,
- Ryutov, D. D. 2007, Plasma Physics and Controlled Fusion, 49, B429
- Ryutov, D. D. 1997, Plasma Physics and Controlled Fusion, 39, A73
- Schumann, W. O. 1952, Zeitschrift Naturforschung Teil A, 7, 149
- Shao, L., & Zhang, B. 2017, PhRvD, 95, 123010
- Terrell, J. 1959, Physical Review, 116, 1041
- Williams, E. R., Faller, J. E., & Hill, H. A. 1971, Physical Review Letters, 26, 721
- Wu, X.-F., Zhang, S.-B., Gao, H., et al. 2016, ApJL, 822, L15
- Yang, Y.-P., & Zhang, B. 2017, ApJ, 842, 23
- Zhang, B., & Li, K. 2018, ApJ, 854, 123

APPENDIX

A. SPHERICAL GEOMETRY

Below we introduce some concepts in spherical geometry, the geometry of a two-dimensional spherical surface, that are used in this paper.

A.1. Great Circle Distance

Let us define (α_1, δ_1) and (α_2, δ_2) as the right ascension and declination in radians of two points 1 and 2 on the sphere, respectively, and $\Delta\alpha$ as the absolute difference in longitude. The angle between the two points θ opened from the center of the sphere is defined by the spherical law of cosines:

$$\theta = \arccos(\sin \delta_1 \sin \delta_2 + \cos \delta_1 \cos \delta_2 \cos(\Delta\alpha)). \quad (\text{A1})$$

This can be straightforwardly derived when one of the poles is used as an auxiliary third point on the sphere.

A.2. Spherical Triangle

Suppose that three points (denoted as 1, 2, 3) on a sphere form a spherical triangle. The three angular distances among the three points (θ_{12} , θ_{13} and θ_{23}) and the measures of the three vertex angles of the triangle ($\angle 132$, $\angle 123$ and $\angle 213$) are related by the cosine rule of the sphere triangle

$$\begin{aligned} \cos \theta_{12} &= \cos \theta_{13} \cos \theta_{23} + \sin \theta_{13} \sin \theta_{23} \cos \angle 132, \\ \cos \theta_{13} &= \cos \theta_{12} \cos \theta_{23} + \sin \theta_{12} \sin \theta_{23} \cos \angle 123, \\ \cos \theta_{23} &= \cos \theta_{12} \cos \theta_{13} + \sin \theta_{12} \sin \theta_{13} \cos \angle 213. \end{aligned} \quad (\text{A2})$$

B. SOLVING THE PARAMETERS OF POSITIONS IN PROBE COMOVING FRAME K'

We adopt a representation of the coordinate transformation in terms of the parameters of rotation — the angle of rotation and the direction cosines of the axis of rotation. The *rotation formula* (Goldstein et al. 2002) is

$$\mathbf{r}' = \mathbf{r} \cos \Phi + \hat{\mathbf{n}}(\hat{\mathbf{n}} \cdot \mathbf{r})(1 - \cos \Phi) + (\hat{\mathbf{n}} \times \mathbf{r}) \sin \Phi, \quad (\text{B3})$$

where Φ is the rotation angle, $\hat{\mathbf{n}}$ is the direction unit vector of axis, \mathbf{r} is the vector of the initial position, and \mathbf{r}' is the vector of the final position.

If one knows the moving direction of the probe (α_0 and δ_0) and the position of a random point (α_1 and δ_1) in the Earth rest Frame K , the corresponding position in the probe comoving Frame K' (α'_1 and δ'_1) must be located at the great circle defined by the moving direction of the probe and the position of the random point in Frame K . In order to calculate the position in Frame K' (α'_1 and δ'_1), one can rotate the cartesian coordinate position vector of the probe moving direction $\mathbf{r}_0 = [\cos \delta_0 \cos \alpha_0, \cos \delta_0 \sin \alpha_0, \sin \delta_0]^T$ by an angle $\Phi = \theta'$ about the axis which is perpendicular to the plane of the great circle and located at the center of the sphere, where θ' can be calculated from Eq. 1. The axis is perpendicular to the plane of the great circle, so that the direction vector of the axis is

$$\mathbf{n} = \begin{bmatrix} n_x \\ n_y \\ n_z \end{bmatrix} = \mathbf{r}_0 \times \mathbf{r}_1 = \begin{bmatrix} \cos \delta_0 \cos \alpha_0 \\ \cos \delta_0 \sin \alpha_0 \\ \sin \delta_0 \end{bmatrix} \times \begin{bmatrix} \cos \delta_1 \cos \alpha_1 \\ \cos \delta_1 \sin \alpha_1 \\ \sin \delta_1 \end{bmatrix} = \begin{bmatrix} \cos \delta_0 \sin \alpha_0 \sin \delta_1 - \cos \delta_1 \sin \alpha_1 \sin \delta_0 \\ \cos \delta_1 \cos \delta_1 \sin \delta_0 - \cos \delta_0 \cos \alpha_0 \sin \delta_1 \\ \cos \delta_0 \cos \alpha_0 \cos \delta_1 \sin \alpha_1 - \cos \delta_1 \cos \alpha_1 \cos \delta_0 \sin \alpha_0 \end{bmatrix}, \quad (\text{B4})$$

where \mathbf{r}_1 is the cartesian coordinate position vector of the random point in Frame K . The direction unit vector is $\hat{\mathbf{n}} = \mathbf{n}/|\mathbf{n}|$. As a result, the cartesian coordinate position vector of the corresponding point \mathbf{r}'_1 in Frame K' can be calculated by Eq.(B3). One can then calculate the celestial position:

$$\alpha'_1 = \arctan \frac{r'_{1y}}{r'_{1x}}, \delta'_1 = \arctan \frac{r'_{1z}}{\sqrt{r'^2_{1x} + r'^2_{1y}}}. \quad (\text{B5})$$

Note that one should pay attention to the quadrant when calculating the celestial positions. One can finally obtain $\sigma_{\alpha'_1}$, $\sigma_{\delta'_1}$ and the correlation coefficient ρ between them.

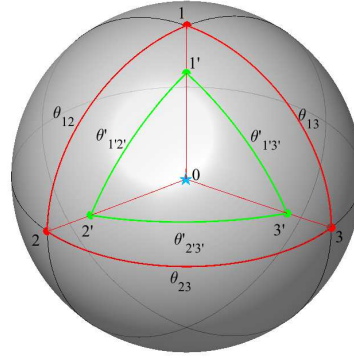


Figure 1. Geometry to solve the motion of the probe. All the points and lines are located on the celestial sphere. The three bright points 1, 2, 3 in Frame K are marked as red points, and their corresponding points $1'$, $2'$, $3'$ in Frame K' are marked as green points. The blue star represents the direction of motion of the probe. Here, the dimensionless velocity is set to $\beta = 0.5$.

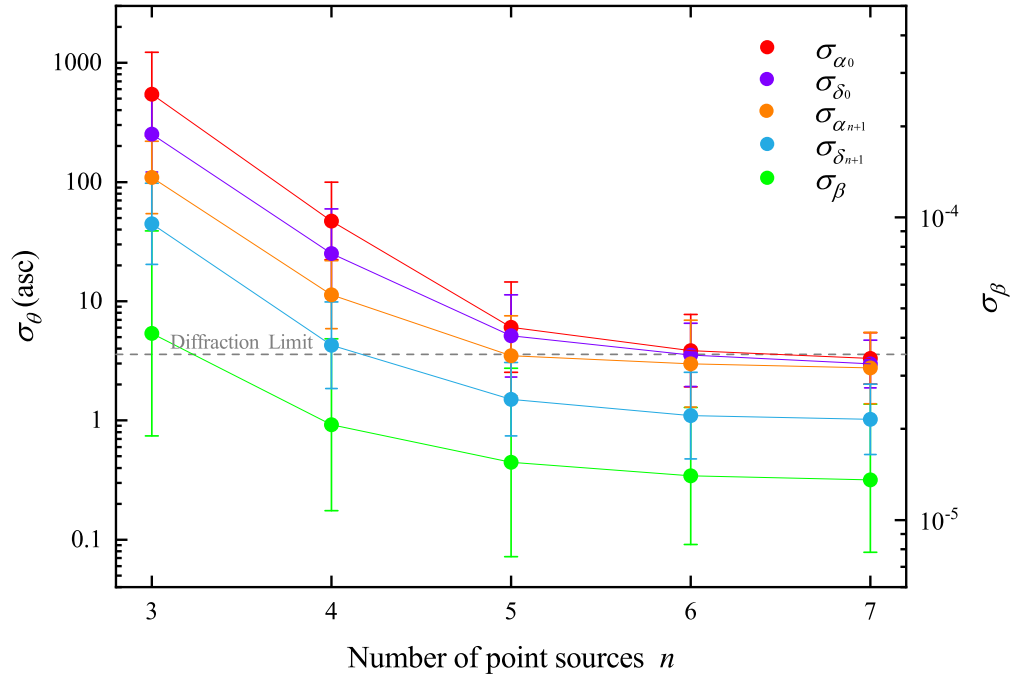


Figure 2. The uncertainties of the moving direction, dimensionless velocity and position of the $(n+1)^{\text{th}}$ as a function of the number of selected sources used to solve the motion of the probe. The red, purple, orange, blue and green circle represent the uncertainties of σ_{α_0} , σ_{δ_0} , $\sigma_{\alpha_{n+1}}$, $\sigma_{\delta_{n+1}}$ and σ_{β} , respectively. All the uncertainties have a decreasing trend as a function of n , even though they converge to certain values as n becomes greater than 5. The diffraction limit can be exceeded for $\sigma_{\alpha_{n+1}}$, $\sigma_{\delta_{n+1}}$ and σ_{β} .

Table 1. Astrometric parameters from *Gaia* DR2

HIP Number ^a	$\alpha^b/^\circ$	$\sigma_\alpha^c/\text{mas}$	$\delta^d/^\circ$	$\sigma_\delta^e/\text{mas}$	G^f/mag
HIP 48002	146.775362659982	0.355484559318881	-65.0719747969472	0.452647622691853	2.7888165
HIP 50099	153.43379086538	0.381048026978585	-70.0378756114751	0.412152102923925	3.1671705
HIP 60260	185.338542066226	0.249153821072983	-60.4007532768981	0.251904680424402	2.972596
HIP 63003	193.648183007381	0.250793038754558	-57.177982492016	0.287536909377994	3.9152856
HIP 65109	200.147396031851	0.866965009254124	-36.7126584300049	0.9151158414171	2.6858432
HIP 68191	209.411620208564	0.110542550229435	-63.6868421732935	0.113597426320103	4.332655
HIP 68413	210.071883961754	0.0157461882226798	-61.4811767464898	0.0212724498777446	6.3933997
HIP 70264	215.654157195748	0.606447518545649	-58.4590342486566	0.645525706923748	4.505525
HIP 70890 ^g	217.393465742603	0.0576531066309365	-62.6761821029238	0.104971236535274	8.953612
HIP 71536	219.471584298892	0.435237848446469	-49.4259545203336	0.43552937583903	4.1545763
HIP 71908	220.624786167374	0.306439160958405	-64.9761453374905	0.346400793582825	3.0168602
HIP 72370	221.965348106629	0.353395987756381	-79.0448239123319	0.249861855221442	3.2268114
HIP 73036	223.892909779778	0.108083930105218	-60.1146530932842	0.107148314251759	4.7807016
HIP 73129	224.18320144613	0.29882749125488	-62.7810549202754	0.28979783900068	6.3000674
HIP 74376	227.983005446366	0.270611403896749	-48.7380355294683	0.257024679570251	3.7678657
HIP 75177	230.451054300018	0.4706870286551	-36.2617424940659	0.430245831516788	2.804096
HIP 75264	230.670180237484	0.627689424158833	-44.6897202575442	0.523389157213469	3.1959176
HIP 79882	244.580739905517	0.611283192789319	-4.69233749011063	0.51437495211855	2.8429356
HIP 80000	244.959020515699	0.408275536496331	-50.1557296301489	0.325488297914412	3.6179643
HIP 82363	252.446811482963	0.281259981504505	-59.0414913798215	0.247374949109005	2.964356
HIP 84405	258.835189375142	0.274003796302741	-26.6077392836698	0.20226466988628	4.795791
HIP 85258	261.324889804672	0.712821224324093	-55.5299930306329	0.705065746762892	2.1833172
HIP 86742	265.867953589588	0.632712365440421	4.56799013350183	0.6014778751505	2.2781103
HIP 86929	266.433176038536	0.247410040661301	-64.7241146561051	0.28347297854899	3.1453683
HIP 92175	281.793608327785	0.379168248663183	-4.74794370906114	0.357594134137972	3.7981637
HIP 93085	284.432655909574	0.564336710740746	-21.1067164143209	0.459084497805038	3.0392666
HIP 95477	291.318920004013	0.463477890459631	-24.5088046123265	0.426221125705944	4.8317966
HIP 96229	293.523230152249	0.181975068418186	7.37826437436815	0.161013880989546	4.0115433
HIP 100345	305.252975453738	0.435907604437754	-14.7814042849006	0.317730995129632	2.7116423
HIP 102488	311.55470104855	0.700139915223491	33.9716578564345	0.812911932858741	2.0226774
HIP 107315	326.046610958014	0.546274241416486	9.87501784822262	0.600684192163677	1.7076352

^aThe star mark from *Hipparcos* catalogue (Perryman et al. 1997)

^bRight ascension at epoch J2015.0

^cStandard uncertainties of right ascension

^dDeclination at epoch J2015.0

^eStandard uncertainties of declination

^fMagnitude in *Gaia*'s unfiltered band

^gProxima

Table 2. Examples of error analysis

β^a	$r^b/^\circ$	$\theta_c^c/^\circ$	D^d/cm	HIP Number ^e	$\sigma_{\alpha_0^f}/10^{2''}$	$\sigma_{\delta_0^g}/10^{2''}$	$\sigma_\beta^h/10^{-5}$	HIP Number ⁱ	$\sigma_{\alpha_4^j}/10^{2''}$	$\sigma_{\delta_4^k}/10^{2''}$	$\theta_{04}^l/^\circ$
0.20	~ 30	~ 0	3.5	HIP 50099	2.755	1.298	1.899	HIP 48002	0.442	0.279	~ 25
				HIP 65109				HIP 75177	0.331	0.207	
				HIP 85258				HIP 86929	0.636	0.185	
0.15	~ 30	~ 0	3.5	HIP 50099	3.345	1.599	1.877	HIP 48002	0.413	0.258	~ 25
				HIP 65109				HIP 75177	0.303	0.194	
				HIP 85258				HIP 86929	0.590	0.171	
0.10	~ 30	~ 0	3.5	HIP 50099	4.564	2.216	1.849	HIP 48002	0.387	0.239	~ 25
				HIP 65109				HIP 75177	0.277	0.182	
				HIP 85258				HIP 86929	0.547	0.159	
0.20	~ 15	~ 0	3.5	HIP 63003	8.183	3.859	4.250	HIP 60260	1.538	0.648	~ 15
				HIP 71536				HIP 71536	1.110	0.701	
				HIP 74376				HIP 82363	1.210	0.762	
0.20	~ 5	~ 0	3.5	HIP 68191	152.837	64.293	18.645	HIP 68413	26.730	12.019	~ 5
				HIP 70264				HIP 73036	26.530	11.601	
				HIP 71908				HIP 73129	28.477	11.605	
0.20	~ 30	~ 45	3.5	HIP 75264	2.051	1.090	5.729	HIP 80000	0.342	0.189	~ 20
				HIP 79882				HIP 84405	0.261	0.191	~ 45
				HIP 95477				HIP 92175	0.270	0.177	~ 70
0.20	~ 30	~ 90	3.5	HIP 86742	0.914	1.150	10.247	HIP 93085	0.253	0.206	~ 60
				HIP 100345				HIP 96229	0.235	0.220	~ 90
				HIP 107315				HIP 102488	0.264	0.191	~ 120
0.20	~ 30	~ 0	35	HIP 50099	0.275	0.130	0.190	HIP 48002	0.042	0.028	~ 25
				HIP 65109				HIP 75177	0.033	0.021	
				HIP 85258				HIP 86929	0.064	0.019	
0.20	~ 30	~ 0	350	HIP 50099	0.028	0.013	0.019	HIP 48002	0.004	0.003	~ 25
				HIP 65109				HIP 75177	0.003	0.002	
				HIP 85258				HIP 86929	0.006	0.002	

^aThe dimensionless velocity

^bRadius of the probe camera's field

^cThe angles between the moving direction of probe and centers of camera's field in Frame K'

^dThe lens' aperture of camera

^eThe star mark of three selected points from *Hipparcos* catalogue (Perryman et al. 1997)

^fStandard uncertainties of right ascension of the moving direction of the probe

^gStandard uncertainties of declination of the moving direction of the probe

^hStandard uncertainties of the dimensionless velocity

ⁱThe star mark of the fourth points from *Hipparcos* catalogue (Perryman et al. 1997)

^jStandard uncertainties of the fourth points' right ascension

^kStandard uncertainties of the fourth points' declination

^lThe angles between the moving direction of the probe and fourth points

Table 3. The motion uncertainties when solving the motion with more than three point sources

n ^a	σ_{α_0} ^b /''	σ_{δ_0} ^c /''	σ_{β} ^d / 10^{-5}	$\sigma_{\alpha'_{n+1}}$ ^e /''	$\sigma_{\delta'_{n+1}}$ ^f /''
3	545.5±441.9	251.5±182.7	4.139±3.231	109.3±76.23	44.55±34.90
4	47.16±35.19	25.19±21.58	2.064±1.350	11.33±7.429	4.283±3.583
5	6.062±5.297	5.126±4.067	1.550±1.110	3.491±2.701	1.507±1.072
6	3.855±2.691	3.543±2.161	1.399±0.730	2.993±2.509	1.100±0.919
7	3.312±1.650	2.975±1.367	1.257±0.767	2.755±1.896	1.022±0.697

^aThe number of selected points sources for solving the motion of the probe

^bStandard uncertainties of right ascension of the moving direction of the probe

^cStandard uncertainties of declination of the moving direction of the probe

^dStandard uncertainties of the dimensionless velocity

^eStandard uncertainties of the $(n + 1)^{\text{th}}$ points' right ascension

^fStandard uncertainties of the $(n + 1)^{\text{th}}$ points' declination